









# Heterojunction of CuO nanoclusters with TiO<sub>2</sub> for photo-oxidation of organic compounds and for hydrogen production

Cite as: J. Chem. Phys. **153**, 034705 (2020); <https://doi.org/10.1063/5.0015277>

Submitted: 29 May 2020 . Accepted: 26 June 2020 . Published Online: 15 July 2020

Maria Guadalupe Méndez-Medrano , Ewa Kowalska , Bunsho Ohtani , Daniel Bahena Uribe ,  
Christophe Colbeau-Justin , Sven Rau , José Luis Rodríguez-López , and Hynd Remita 



View Online



Export Citation



CrossMark

Lock-in Amplifiers  
up to 600 MHz



Watch



# Heterojunction of CuO nanoclusters with TiO<sub>2</sub> for photo-oxidation of organic compounds and for hydrogen production

Cite as: J. Chem. Phys. 153, 034705 (2020); doi: 10.1063/5.0015277

Submitted: 29 May 2020 • Accepted: 26 June 2020 •

Published Online: 15 July 2020



View Online



Export Citation



CrossMark

Maria Guadalupe Méndez-Medrano,<sup>1,2</sup> Ewa Kowalska,<sup>3</sup> Bunsho Ohtani,<sup>3</sup> Daniel Bahena Uribe,<sup>4</sup> Christophe Colbeau-Justin,<sup>1</sup> Sven Rau,<sup>5</sup> José Luis Rodríguez-López,<sup>2,a)</sup> and Hynd Remita<sup>1,6,b)</sup>

## AFFILIATIONS

<sup>1</sup>Institut de Chimie Physique, UMR 8000 CNRS, Université Paris-Saclay, 91405 Orsay, France

<sup>2</sup>Advanced Materials Department, IPICYT, 78216 San Luis Potosi, SLP, Mexico

<sup>3</sup>Institute for Catalysis, Hokkaido University, Sapporo 001-0021, Japan

<sup>4</sup>Centro de Investigación y de Estudios Avanzados del Instituto Politécnico Nacional, I07360 Mexico City, D.F., Mexico

<sup>5</sup>Institute for Inorganic Chemistry 1, Ulm University, Albert-Einstein-Allee 11, 89081 Ulm, Germany

<sup>6</sup>CNRS, Institut de Chimie Physique, UMR 8000, 91405 Orsay, France

**Note:** This paper is part of the JCP Special Topic on Photocatalysis and Photoelectrochemistry.

**a)** Email: [jlrdez@ipicyt.edu.mx](mailto:jlrdez@ipicyt.edu.mx). Tel.: +52 444 834 2000 x 7217

**b)** Author to whom correspondence should be addressed: [hynd.remita@universite-paris-saclay.fr](mailto:hynd.remita@universite-paris-saclay.fr). Tel.: +33 (0)1 69 15 72 58

## ABSTRACT

Heterojunctions of small CuO nanoclusters (synthesized by radiolysis) with TiO<sub>2</sub> (commercial P25) induced a photocatalytic activity under visible light irradiation in a wide range of wavelengths due to the narrow bandgap of CuO nanoclusters of around 1.7 eV. The optical, chemical, and electrical properties of these composite nanomaterials were studied. The photocatalytic properties of bare and modified TiO<sub>2</sub>-P25 were studied for water purification (photooxidation of organic compounds such as phenol and 2-propanol) and for hydrogen generation under visible light irradiation. Time resolved microwave conductivity signals showed activation of TiO<sub>2</sub> under visible light, proving the injection of electrons from CuO nanoclusters to the conduction band of TiO<sub>2</sub>-P25. The modified materials showed high photocatalytic activity under visible light. The important role of charge-carriers was demonstrated for both photoreduction and photooxidation reactions.

Published under license by AIP Publishing. <https://doi.org/10.1063/5.0015277>

## I. INTRODUCTION

Titanium dioxide (TiO<sub>2</sub>) is currently the most widely used photocatalyst because of its high photocatalytic activity, chemical and thermal stability, large scale production, low cost, and low-toxicity.<sup>1-3</sup> TiO<sub>2</sub> is an excellent photocatalyst for the decomposition of many organic compounds, and TiO<sub>2</sub> modified with metal nanoparticles (e.g., Cu, Au, Ag, and Pt) can be efficient for hydrogen generation by alcohol dehydrogenation.<sup>4,5</sup> However, TiO<sub>2</sub> also has some drawbacks: (1) a high rate of charge-carrier recombinations, which leads to a low quantum efficiency and (2) a high value of the energy bandgap for its crystalline phases (e.g., 3.2 eV and 3.1 eV for anatase and rutile, respectively),<sup>6</sup> which means that it can only

be excited under UV or near-UV.<sup>7</sup> However, the solar spectrum is composed of only ~4% of UV light. Therefore, a lot of research is focused on the development of visible-light responsive photocatalysts for a more efficient use of solar energy for energy conversion, hydrogen production by the water splitting process (PWS),<sup>4,8</sup> CO<sub>2</sub> reduction,<sup>9</sup> and water and air treatment.<sup>10,11</sup>

To enhance its photocatalytic activity under UV and visible light, TiO<sub>2</sub> has been doped with cations and ions of various elements (e.g., N, C, S, . . .), surface modified with metal nanoparticles (such as Au, Ag, Pt, . . .), or associated with other semiconductors (SCs) (such as ZrO, ZnS, CdS, BiOCl, BiOBr, and WO<sub>3</sub>).<sup>12</sup> The heterojunctions with another semiconductor of a narrow bandgap (NBG-SC) can lead to some advantages such as (i) photoactivity under visible

irradiation, (ii) better charge carrier separation,<sup>13</sup> (iii) lower cost than metal modification, and (iv) possible co-catalytic reactions.<sup>14</sup>

Less expensive materials like copper-based nanomaterials have attracted attention in the field of photocatalysis.<sup>10,15–17</sup> It has been proposed that coupling of TiO<sub>2</sub> (*n*-type semiconductor) with copper oxide (*p*-type semiconductor) of a narrow bandgap (1.7 eV)<sup>18</sup> could overcome the limitations of TiO<sub>2</sub> in terms of visible light absorption and charge-carrier recombinations, enhancing the photoactivity under UV irradiation, principally under visible irradiation. However, it should be pointed out that titania modification with Cu-based bimetallic nanoparticles (NPs), for example, Cu–Ag, Cu–Au, and Cu–Pt,<sup>10,15–17</sup> does not always lead to an improvement in the photocatalytic activity. For example, it has been proposed that the deposition of two metals close to each other (e.g., core–shell nanostructures) can result in charge carrier recombination (electron transfer between metallic deposits) instead of “hot” electron transfer from plasmonic metal nanoparticles (Ag–Cu and Ag–Au NPs) to the conduction band (CB) of titania.<sup>19,20</sup>

Copper has recently attracted a lot of attention because of its low cost, good conductivity, and excellent antibacterial and antifungal properties. Recent studies have reported the promising activity of Cu-based NPs as catalysts for hydrogen production and CO<sub>2</sub> reduction by photocatalysis.<sup>4,21–23</sup> Xu and Sun showed significant photoactivity of TiO<sub>2</sub> modified with CuO nanoparticles for H<sub>2</sub> generation from a water/methanol solution mixture.<sup>14</sup> In that study, the photocatalytic activity of CuO/TiO<sub>2</sub> was even higher than that of Pt/TiO<sub>2</sub>, and CuO nanoparticles worked as electron scavengers and co-catalysts for hydrogen production.<sup>14</sup> Other studies also reported that CuO/TiO<sub>2</sub> is also an efficient photocatalyst for waste water treatment in the degradation of organic pollutants under visible light.<sup>13,24,25</sup>

Several chemical and physical routes have been used to prepare TiO<sub>2</sub>-based composites. In aqueous solution, the methods of preparation involve the impregnation method,<sup>14</sup> sol–gel, hydrothermal methods, and ionizing radiations ( $\gamma$ -rays, x rays, or electron or ion beams). Radiolysis is a very efficient technique to synthesize metal nanoparticles in solutions or on supports.<sup>26–29</sup> The radiolytic method presents the advantage of using simple physicochemical conditions, such as atmospheric pressure and room temperature, and of absence of contaminants. The method results in homogeneous reduction and nucleation, leading to metal nanoparticles of controlled size.<sup>30</sup>

In this work, CuO nanoclusters (with different loadings of Cu: 0.5 wt.%–2 wt.%) have been synthesized on TiO<sub>2</sub> by radiolysis (gamma irradiation). The composite CuO–TiO<sub>2</sub> photocatalyst presents high photocatalytic activity under UV and, more interestingly, under visible light. Time resolved microwave conductivity (TRMC) signals show that CuO nanoclusters, when excited by visible light, inject electrons in the conduction band of TiO<sub>2</sub>, inducing a high photoactivity for organic pollutant degradation and hydrogen production in a water/methanol mixture.

## II. EXPERIMENTAL

### A. Materials

As the support material, titanium(IV) oxide (TiO<sub>2</sub>), provided by Evonik [Commercial TiO<sub>2</sub>–P25, with 50 m<sup>2</sup> g<sup>−1</sup> of surface

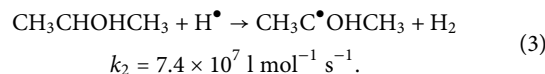
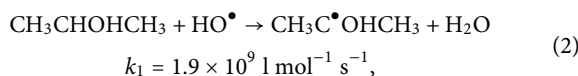
area and a crystalline composition of anatase (73%–85%), rutile (14%–17%), and amorphous titania (0%–13%)<sup>31</sup>], was used. Cupric sulfate (CuSO<sub>4</sub>, Sigma, purity  $\approx$ 99%) was used as the precursor to obtain Cu-based nanoclusters. Phenol (C<sub>6</sub>H<sub>5</sub>OH, Fulka), 2-propanol [CH<sub>3</sub>CH(OH)CH<sub>3</sub>, Sigma-Aldrich, 99.5%], methanol (CH<sub>3</sub>OH, ACS reagent,  $\geq$ 99.8%), acetic acid (CH<sub>3</sub>COOH, Wako, 99.7%), and deionized water (Milli-Q with 18.6 M $\Omega$ ) were used.

### B. Photocatalyst preparation: Modification of TiO<sub>2</sub>–P25 by radiolysis

Photocatalysts were synthesized by radiolytic reduction of Cu<sup>2+</sup> ions. TiO<sub>2</sub>–P25 was placed in suspensions of aqueous solutions containing Cu<sup>2+</sup> (1  $\times$  10<sup>−3</sup>M) (the loading of copper was 0.5 wt.%, 1 wt.%, and 2 wt.%) and 2-propanol (0.1M) (used to scavenge oxidizing HO $\bullet$  radicals generated by water radiolysis).<sup>32</sup> The suspensions were deaerated with nitrogen gas under stirring for 20 min and then irradiated for 3.5 h with a <sup>60</sup>Co panoramic gamma source with a dose rate of 2.3 kGy h<sup>−1</sup> (dose = 8 kGy). When the aqueous solutions are irradiated by high energy radiation such as  $\gamma$ -rays, X rays, or electron beam excitation, ionization of water takes place as follows:<sup>33</sup>



Indeed, high energy radiation of water leads to the formation of solvated electrons ( $e_s^-$ ), which are strong reducing species [ $E^0(\text{H}_2\text{O}/e_s^-) = -2.87\text{V}_{\text{NHE}}$ ], and free radicals—H $\bullet$  [ $E^0(\text{H}^+/\text{H}^\bullet) = -2.3\text{V}_{\text{NHE}}$ ] and HO $\bullet$  [ $E^0(\text{HO}^\bullet/\text{H}_2\text{O}) = +2.8\text{V}_{\text{NHE}}$ ].<sup>32</sup> Strong oxidative hydroxyl radicals HO $\bullet$  [ $E^0(\bullet\text{OH}/\text{H}_2\text{O}) = +2.34\text{V}_{\text{NHE}}$  at pH 7] are also generated.<sup>34</sup> Alcohol (such as 2-propanol) is added to the solutions to scavenge oxidation hydroxyl radicals, leading to formation of alcohol reducing radicals,<sup>26,33</sup>



The alcohol radicals formed by reactions (2) and (3) are reducing agents:  $E^0((\text{CH}_3)_2\text{CO}/(\text{CH}_3)_2\text{C}^\bullet\text{OH}) = -1.8\text{V}_{\text{NHE}}$  at pH 7. Therefore, these secondary radicals are able to directly reduce metal ions with mono- and multi-valence into zero valence. Cu<sup>2+</sup> ions are reduced on TiO<sub>2</sub> by  $e_s^-$  and (CH<sub>3</sub>)<sub>2</sub>C $\bullet$ OH radicals induced by solvent radiolysis.<sup>29,35</sup> Solvent radiolysis generates a homogeneous distribution of solvated electrons and reducing radicals, leading to homogeneous reduction and nucleation. Therefore, metal nanoparticles of homogeneous size are obtained.<sup>26,32</sup> The radiolytic reduction mechanisms of copper ions have been already described in other publications.<sup>35</sup> The dose used for irradiation is the dose necessary to reduce Cu<sup>II</sup> into Cu<sup>0</sup> on TiO<sub>2</sub>. At this dose, TiO<sub>2</sub> is not affected by irradiation, and there is no reduction of Ti<sup>IV+</sup>. The Cu<sup>0</sup> clusters formed on TiO<sub>2</sub> will be oxidized when in contact with air. It is known that copper nanoclusters are sensitive to oxygen and are oxidized in air very fast, leading to formation of small CuO clusters.<sup>26,35–37</sup>

The Cu-modified TiO<sub>2</sub>-P25 photocatalysts were separated by centrifugation and dried at 60 °C for 18 h. The supernatant was completely transparent after centrifugation, indicating that all Cu-based nanoclusters were deposited on TiO<sub>2</sub>-P25.<sup>26,32</sup> The modified materials present a light green color. The samples were labeled P25 and CuO<sub>x</sub>/P25, where x is the mass loading in copper.

### C. Material characterization

The heterojunction CuO@TiO<sub>2</sub> was characterized by high angle annular dark field scanning transmission electron microscopy (HAADF-STEM). For observation, the samples were dispersed in 2-propanol by sonication and then dropped on gold coated holey carbon grids. We used a Cs corrected JEOL-ARM-200F electron transmission microscope at 200 kV. Line-scan profile energy-dispersive x-ray spectroscopy (EDS) measurements were obtained with an Oxford detector.

For x-ray photoelectron spectroscopy (XPS) analysis, the samples were deposited on fully covered carbon films in order to avoid powder release at pressure lower than 10<sup>-7</sup> Torr on the analysis chamber. High resolution scans were taken for five elements, and the number of scans differed depending on each element content in the sample, i.e., 50 scans were taken for Ti and O, 100 scans for C, and 300–500 scans for Cu using a JEOL JPS-9010MC with Mg K $\alpha$  radiation and a hemispherical electron energy analyzer.

For diffuse reflectance spectroscopy (DRS), Cary 5000, a UV-Vis-NIR spectrophotometer equipped with an integrating sphere from Agilent Technologies, was used with KBr as the reference sample.

For time resolved microwave conductivity (TRMC) measurements, EKSPLA [a pulsed and tunable (220 nm–2000 nm) laser source with an optical parametric oscillator (OPO)], NT342B, and a microwave generated by a Gunn diode (30 GHz) were used. This technique used to study the dynamics of photogenerated charge-carriers under UV and visible irradiation was described in previous papers.<sup>5,6,15</sup>

### D. Photocatalytic activity test

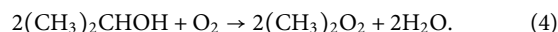
#### 1. Phenol degradation under visible light

Phenol was used as the model pollutant in water (C<sub>6</sub>H<sub>5</sub>OH, 50 ppm). Its photodecomposition was studied in a 10-mm light path quartz cell reactor containing 3.5 mL of phenol solution and 1 g L<sup>-1</sup> of the photocatalyst. The photocatalyst was dispersed in the solution by sonication and kept under stirring for 10 min under dark conditions to reach equilibrium between adsorption and desorption. Then, the solutions were irradiated with a xenon lamp (Oriel 300 W), and a cut-off filter (AM-32603-1, LOT-Oriel) ( $\lambda > 450$  nm) was used. The photocatalytic tests were conducted under oxygen bubbling at a fixed rate flow.

Sampled aliquots of 0.5 ml were taken from the irradiated suspensions at different time intervals. The catalyst powders were separated from the solutions by centrifugation. The solutions were analyzed by high performance liquid chromatography (HPLC, Agilent 1260 infinity quaternary LC) equipped with a UV-detector set at 260 nm for phenol analysis. An isocratic mobile phase consisted of 80% H<sub>2</sub>O and 20% acetonitrile (ACN) for elution at 1 mL min<sup>-1</sup> flow rate.

#### 2. 2-propanol degradation under visible irradiation

The photodecomposition of 2-propanol was carried out in a reactor, where 15 mL of the liquid suspension containing 50 mg of photocatalyst was dispersed in 5 mL of 2-propanol (5 vol. %), which was covered with a septum to avoid evaporation of acetone. The photocatalyst was irradiated for 3 h using a xenon lamp and a cut-off filter (Y48, Asahi Techno Glass) with wavelengths above 450 nm ( $\lambda \geq 450$  nm) and under magnetic stirring (1000 rpm). To control the reaction temperature at 25 °C, the reactor was immersed into a water bath. Every hour, the sample was taken from the reactor, filtered using Whatman Mini-UniPrep PVDF filters, and analyzed by using a gas chromatograph equipped with a flame ionization detector (GC-FID; Shimadzu GC-14B). This reaction was followed by acetone generation, according to the reaction<sup>38</sup>



#### 3. Photocatalytic production of hydrogen (H<sub>2</sub>)

The photocatalytic reduction reaction was performed through methanol dehydrogenation (H<sub>2</sub> evolution) in a closed Pyrex glass reactor. 2 mg of each photocatalyst was suspended in 2 mL of degassed aqueous solution containing 25 vol. % of methanol (used as a sacrificial agent) added under an argon atmosphere. The photocatalyst was dispersed in the solution by sonication for 30 s and kept under vigorous stirring. The quantity of hydrogen produced was determined by a Bruker Scion GC/MS gas chromatograph (GC) with a column: Mol. Sieve 5 A 75 m  $\times$  0.53 mm I.D., flow rate 22.5 mL min<sup>-1</sup>, oven temp. 70 °C, and detector temperature 200 °C under argon carrier gas. LEDs (Innotas Elektronik) with wavelengths of 400 nm and 470 nm were used as irradiation sources.

#### 4. Study of stability under visible light

The stability of the photocatalysts with cycling was analyzed for the photodecomposition of phenol. The resultant supernatants (aliquots of 1 mL at different irradiation times and for different cycles for 8 h irradiation) were analyzed by HPLC. The powder after different cycles was dried at 60 °C overnight, and the collected samples were weighed and reused (1 mg/1 ml ratio) after each cycle.

## III. RESULTS AND DISCUSSION

STEM observations of the modified titania show small Cu-based nanoclusters (around 1–3 nm) homogeneously dispersed on the surface of the TiO<sub>2</sub>-P25, as shown in Fig. 1. Similar sizes of CuO nanoclusters were observed for the samples with 1% and 2% loadings. The HAADF-STEM images for Cu-based nanoclusters show arrangements of crystallographic planes, corresponding to CuO. Crystallographic planes and FFT (fast Fourier transformation) can be observed. The measure of the interplanar spacing ( $d$ ) was found to be equal to 0.2 nm, which corresponds to the interplanar distance for (11-1) planes of CuO, according to JCPDS file No. 48-1548.<sup>39</sup>

The composition of CuO-nanoclusters was determined by STEM-electron dispersive x-ray spectroscopy (EDS). Different clusters were analyzed. The line profile spectra across the different individual nanoclusters show the presence of Cu (L and K) as well as Au (L and M) from the grids (Fig. S1).

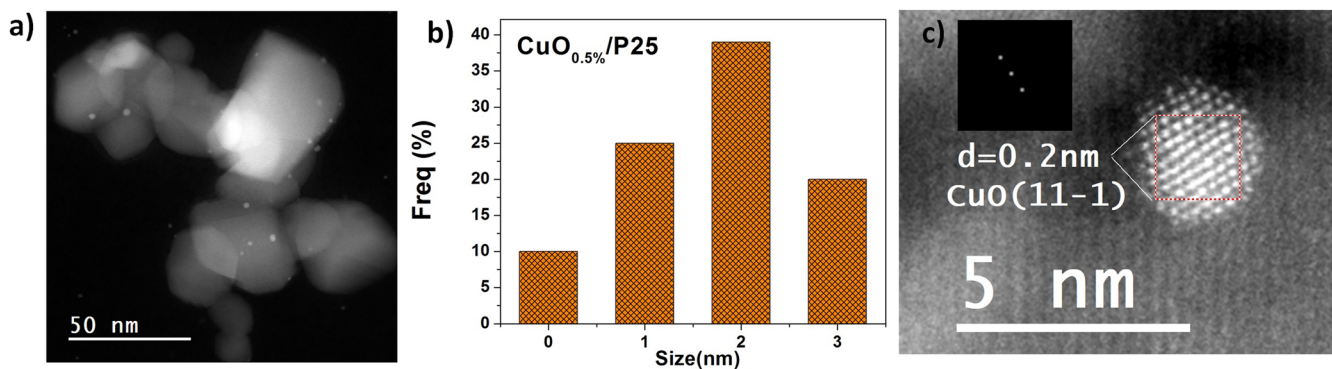


**FIG. 1.** TEM images of (a)  $\text{CuO}_{0.5\%}/\text{P25}$  with (b) the corresponding histogram of the size distribution of CuO nanoclusters and (c) HAADF-STEM of BF-STEM images of  $\text{CuO}_{0.5\%}/\text{P25}$  with FFT (fast Fourier transform) images for the planes of CuO.

The analysis of the chemical composition of the modified  $\text{TiO}_2$ -P25 was carried out by XPS. The core level signals of Cu, Ti, O, and C were observed. The results are presented in Fig. S2 and Table S1. Characterization by XPS demonstrates the presence of  $\text{Ti}2p$  peaks, characteristic of  $\text{Ti}^{4+}$  in  $\text{TiO}_2$ , at 459.8 eV and 465.6 eV related to  $\text{Ti}2p_{3/2}$  and  $\text{Ti}2p_{1/2}$  orbitals; other peaks at 531.2 eV are attributed to  $\text{O}1s$  of  $\text{TiO}_2$ , and an additional peak at 284.8 eV is attributed to  $\text{C}1s$  peaks (the signal obtained from the carbon films). In Cu core peaks, two components  $\text{Cu}2p_{1/2}$  and  $\text{Cu}2p_{3/2}$  are observed.<sup>40</sup> Concerning  $\text{Cu}2p_{3/2}$  core levels, the  $E_B$  positions are in the range of 933.4 eV. The copper position range agrees with the  $\text{Cu}^{2+}$  chemical state, but the characteristic shake-up of  $\text{Cu}^{\text{II}}$  ions is naught or very weak. The shake-up decreases with the reduction of  $\text{Cu}^{\text{II}}$  (into  $\text{Cu}^{\text{I}}$  and  $\text{Cu}^0$ ) but is also sensitive to the particle size of  $\text{Cu}^{\text{II}}$ -based NPs.<sup>41</sup> Previous studies have reported that the energy position of the rising Cu K-edge of the XANES spectra of these nanoclusters corresponds to  $\text{Cu}^{\text{II}}$  species.<sup>15</sup>

The DRS spectra of the modified samples exhibit a slight shift in the absorption toward visible light, compared with  $\text{TiO}_2$ -P25 that presents an absorption around 400 nm,<sup>42</sup> as shown in Fig. 2. This shift is related to the equilibrium of the conduction band of  $\text{TiO}_2$ -P25 by the junction with the CuO-nanoclusters. These nanoclusters are responsible for the large absorption band in the IR with a maximum at 800 nm related to  $2E_g \rightarrow 2T_{2g}$  inter-band transitions in the  $\text{Cu}^{\text{II}}$ -based clusters on  $\text{TiO}_2$ .<sup>43</sup> This absorption results in a light green color of the samples.

The TRMC signals are shown in Fig. 3. The samples were excited at fixed wavelengths under visible regions 450 nm, 480 nm, and 550 nm.  $\text{TiO}_2$ -P25 modified with CuO-nanoclusters exhibits strong TRMC signals under visible light. These samples exhibit higher  $I_{\text{max}}$  values than bare  $\text{TiO}_2$ -P25 excited with wavelengths within the visible range (450 nm, 480 nm, and 550 nm). At 450 nm, all CuO containing samples show signals at similar  $I_{\text{max}}$  values. However, the samples show different signal decays. The decay is slower with a decrease in the amount of CuO, indicating that the recombination of photogenerated charge-carriers is slower. At 480 nm, the samples still present signals with similar  $I_{\text{max}}$  values and signal decay.

However, at 550 nm, the  $I_{\text{max}}$  value of the signals increases with CuO loading. The signal decrease with Cu0.5% is slower, indicating more charge carriers in this sample.

These TRMC results shed light on the photocatalytic mechanisms involved in  $\text{TiO}_2$ -P25 modified with CuO-nanoclusters under visible light irradiation due to its narrow bandgap (1.7 eV).<sup>18</sup> TRMC signals are higher with Cu- $\text{TiO}_2$  samples excited under visible light, indicating higher charge carriers and more electrons in the CB of  $\text{TiO}_2$ . The CuO-nanoclusters attached at the surface are able to activate the  $\text{TiO}_2$  photocatalyst through a heterojunction between  $p$ -type CuO and  $n$ -type  $\text{TiO}_2$  [Fig. 3(d)]. Depending on the band positions of these two semiconductors and the formed heterojunction, the photoexcited electrons are transferred from the CB of CuO to the CB of  $\text{TiO}_2$  until the Fermi levels of the semiconductors reach the same value. Electron transfer between the semiconductors is due

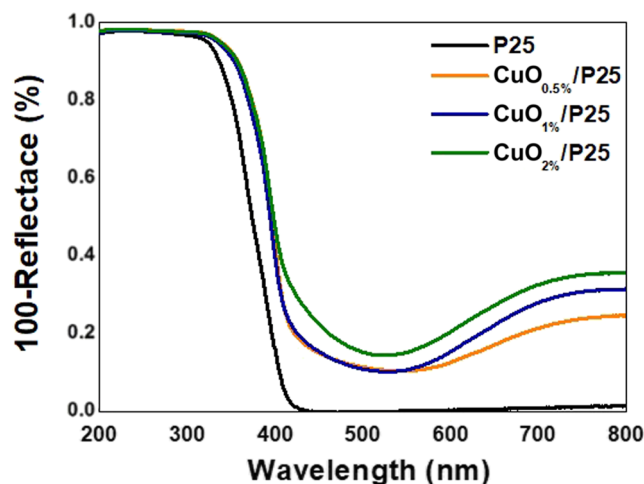
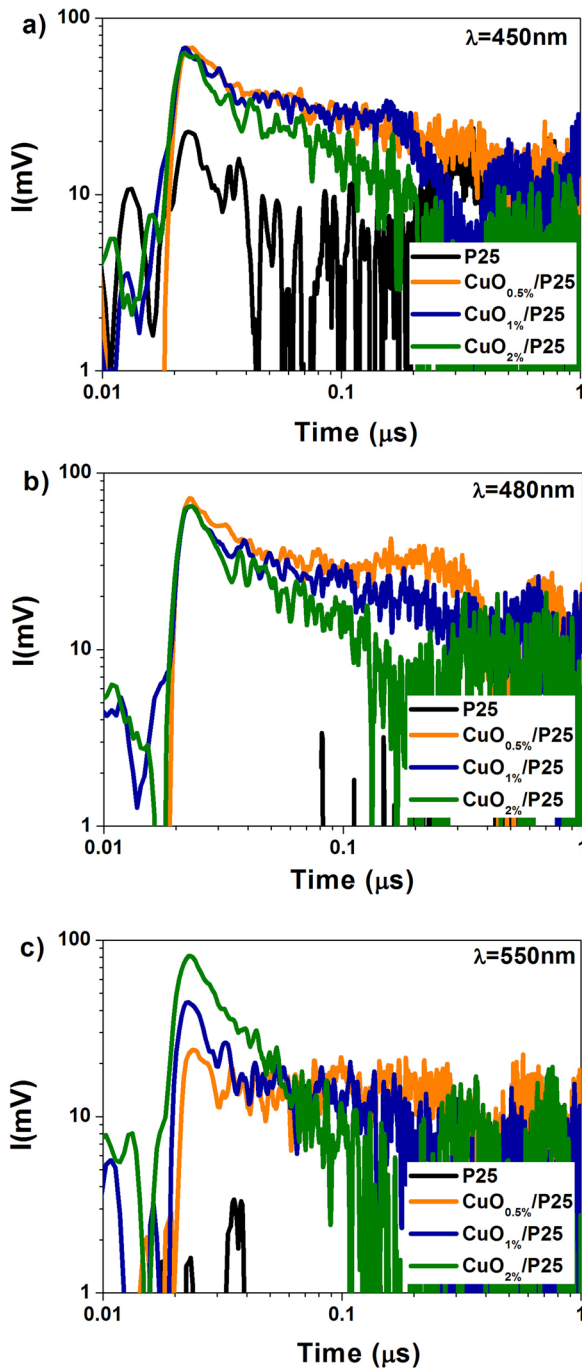
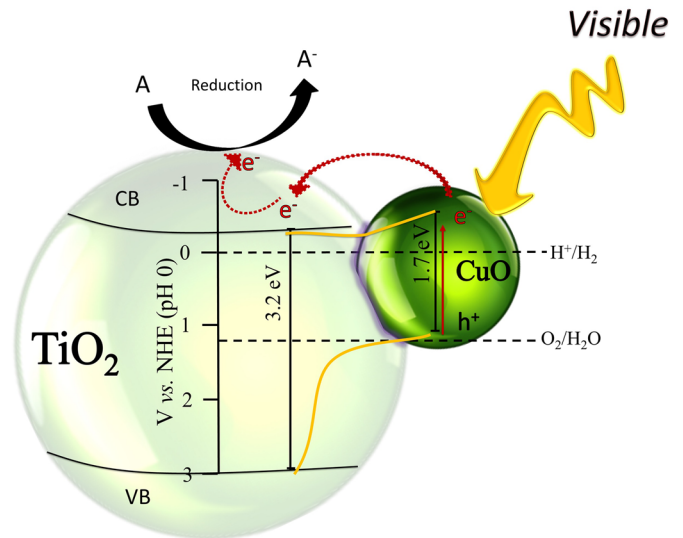


**FIG. 2.** UV-Vis diffused reflectance spectra of  $\text{TiO}_2$ -P25 and modified  $\text{TiO}_2$ -P25 with different loadings in CuO-nanoclusters.



Heterojunction of p-type CuO and n-type TiO<sub>2</sub>



Interfacial charge-transfer excitation

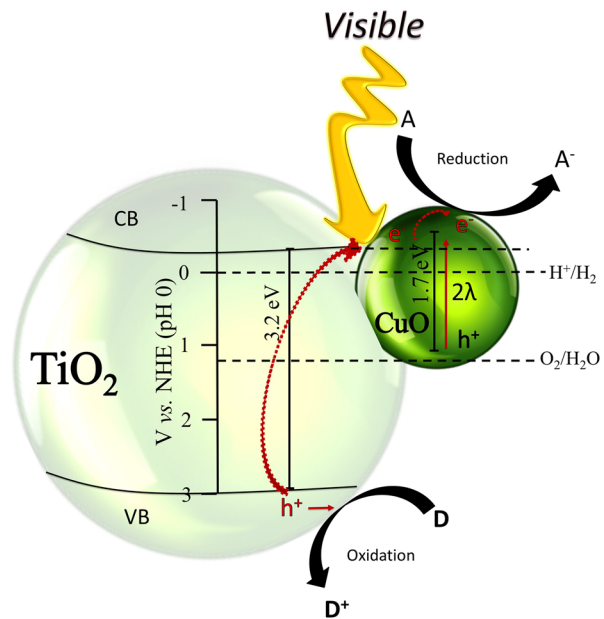


**FIG. 3.** TRMC signals of bare and modified TiO<sub>2</sub>-P25 with different loadings in CuO-nanoclusters after excitation at different wavelengths: (a) 450 nm, (b) 480 nm, and (c) 550 nm; the corresponding laser energies were 6.1 mJ cm<sup>-2</sup>, 5.8 mJ cm<sup>-2</sup>, and 4.5 mJ cm<sup>-2</sup>, respectively, and [(d) and (e)] the mechanisms proposed for TiO<sub>2</sub>-P25 modified with CuO-nanoclusters under visible light.

to the favorable energetics of the relative positions of the CBs, reducing the electron-hole recombination probability significantly and increasing electron lifetime. In this case, hot electrons transferred to TiO<sub>2</sub> can then reduce electron acceptors to drive photocatalytic

reactions. The positive holes remaining in CuO have almost no oxidation ability because the VB level in CuO is more cathodic than the VB of TiO<sub>2</sub>, and therefore, it is impossible to expect these positive holes to be active. It has to be noted that the energy bandgap value

decreases with the size of CuO clusters. Ge *et al.* reported that their bandgap decreases from 2.6 eV to 1.4 eV when their size increases from 1.1 nm to 2 nm.<sup>44</sup>

Another possible mechanism reported by Irie *et al.* is that through interfacial charge transfer (IFCT) [Fig. 3(e)], electrons in the VB of TiO<sub>2</sub> can be excited and injected into the CB of CuO.<sup>45,46</sup> In this case, the CB in TiO<sub>2</sub> is only slightly higher than the oxygen-reduction potential, and excited electrons in CuO may not reduce electron acceptors in the one-electron reduction mode. In this case, two-electron reduction of oxygen may happen to induce visible-light photocatalysis, and active holes created in the VB of TiO<sub>2</sub> oxidize the electron donors. This mechanism is less likely because it would lead to trapped charge carriers and lower TRMC signals with Cu-TiO<sub>2</sub> samples, while the contrary is observed.

CuO activates TiO<sub>2</sub> in a wide range of wavelengths under visible light irradiation, inducing a higher photocatalytic activity in the visible region.

#### IV. PHOTOCATALYTIC TESTS

##### A. Phenol and 2-propanol degradation under visible light irradiation

The photoactivity of the samples was tested for hydrogen production and degradation of model pollutants (phenol and 2-propanol) under visible light.

The photodegradation curves of phenol and 2-propanol (by acetone production) are shown in Fig. 4. For the phenol degradation process, it is well-known that by photocatalysis, complete mineralization is obtained.<sup>47</sup> The phenol degradation rate with irradiation time is shown in Fig. 4(a). A clear enhancement in the photoactivity of TiO<sub>2</sub>-P25 was observed under visible light irradiation (wavelengths higher than 450 nm). The photoactivity depends on the loading with CuO clusters, and the best performance is obtained with low loading in CuO-nanoclusters for the Cu<sub>0.5%</sub>/P25 sample. The photoactivity of bare TiO<sub>2</sub>-P25 under visible light is usually very low because the illumination energy is lower than its bandgap energy,

and its low photoactivity is related to the presence of a rutile phase in TiO<sub>2</sub>-P25.<sup>31</sup>

For 2-propanol degradation [Fig. 4(b)], only acetone is detected as intermediate, as shown in Eq. (1). Here, again, the modification with a lower amount of CuO (0.5%) leads to a slightly higher photocatalytic activity than the modification with 1% and 2% of CuO-nanoclusters. Surface modification with copper oxide nanoclusters induces a modification of the absorption properties of the TiO<sub>2</sub>-P25 and particularly an enhancement in the absorption in the visible range, creating an activity under visible light.

It is clear that, for photooxidation of organic compounds, higher photoactivity is obtained with a smaller amount of CuO nanoclusters. In addition, this photocatalytic response can be correlated with the TRMC signals of the photocatalysts previously discussed. The CuO<sub>0.5%</sub>/P25 samples showed the highest  $I_{max}$  value (compared to that obtained with bare TiO<sub>2</sub>-P25) at 450 nm, which represents more electrons in the conduction band of the semiconductor TiO<sub>2</sub>. In addition, for CuO<sub>0.5%</sub>/P25, the decrease in the signal is lower, which refers to a low recombination process and more charge carriers.

##### B. Photocatalytic hydrogen generation

Injected electrons in the conduction band of TiO<sub>2</sub> can reduce H<sup>+</sup> into H<sub>2</sub>, while the holes on the surface of the semiconductor are scavenged by the methanol present in the solution. Methanol reacts with the photo-generated holes, thus decreasing the charge carriers' recombination rate and enhancing the photocatalytic production of hydrogen by two processes: (i) H<sup>+</sup> reduction and (ii) methanol dehydrogenation.<sup>48,49</sup> Hydrogen production tests under visible light at  $\lambda = 470$  nm (results shown in Fig. 5) confirm that modification of TiO<sub>2</sub> with small CuO-nanoclusters induces its activation under visible light. Almost no hydrogen is detected with bare TiO<sub>2</sub>-P25 and CuO<sub>0.5%</sub>/P25. However, with a higher loading in CuO, hydrogen generation increases. It has to be noticed that CuO<sub>0.5%</sub>/P25 was the best sample for photooxidation/degradation of organic compounds. This can be explained by TRMC analysis, which

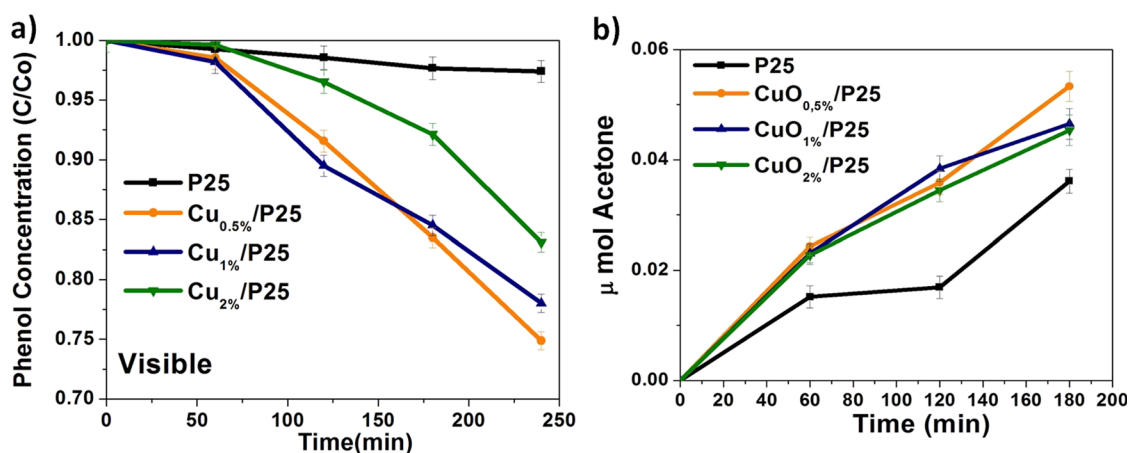


FIG. 4. (a) Degradation curve of phenol under visible light irradiation >450 nm and (b) 2-propanol degradation followed by the amount of acetone generated under visible light >450 nm with bare TiO<sub>2</sub>-P25 and TiO<sub>2</sub>-P25 modified with different loadings of CuO-nanoclusters.

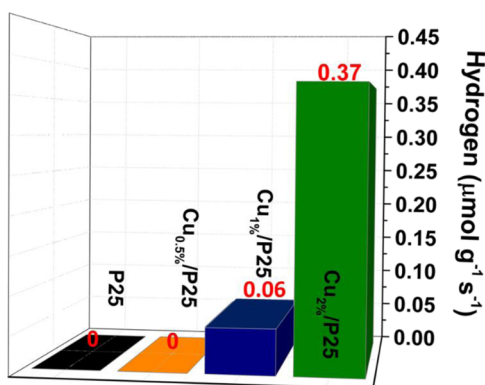


FIG. 5. Photochemical H<sub>2</sub> generated with an LED at  $\lambda = 470$  nm with bare and CuO-modified TiO<sub>2</sub>-P25 after 4 h irradiation.

shows different behaviors of electron injection depending of the wavelength excitation. For CuO<sub>0.5%</sub>/P25, more electrons are injected at lower wavelengths in the CB of TiO<sub>2</sub>, while for CuO<sub>1%</sub>/P25 and CuO<sub>2%</sub>/P25, more injections of electrons are obtained at higher wavelengths. CuO nanoclusters can undergo possible reduction during hydrogen production reaction to zero-valent copper. Indeed, previous studies have shown that the Cu<sup>2+</sup> species are reduced to Cu<sup>1+</sup> during the hydrogen generation process, and after irradiation time, the formation of zero-valent copper occurs.<sup>50</sup> This previous study on copper-modified TiO<sub>2</sub> and ZrTiO<sub>4</sub> points out that the photocatalysts undergo dramatic modifications, leading to the real working systems being quite different from the starting ones.<sup>50</sup> H<sub>2</sub> evolution can be explained by a synergic effect due to the presence of the CuO (or Cu<sub>2</sub>O)/TiO<sub>2</sub> heterojunction and metallic copper clusters.

### C. Stability with cycling

The stability of the photocatalysts after cycling under visible light ( $\lambda \geq 450$  nm) was studied for phenol degradation [see Fig. S3(a) for the sample CuO<sub>0.5%</sub>/P25]. The photoactivity decreases after three cycles. The samples were characterized after three cycles. XPS analysis shows that the peaks corresponding to the binding energy of Cu<sub>2p</sub> core levels decrease (before disappearing) with cycling [Fig. S3(b)]. STEM images [Figs. S3(c)–S3(e)] show that (3 cycles) after the second cycle, some aggregations of Cu-based nanoclusters were observed, whereas after the third cycle, TiO<sub>2</sub> was free of CuO nanoparticles; thus, leaching of Cu was proved [Fig. S3(e)]. It is known that Cu nanoclusters are not stable at nanoscale. The loss of Cu<sub>2p</sub> XPS signals and a decrease in the photocatalytic activity are due to Cu leaching. Moreover, copper oxides are susceptible to photocorrosion (in contrast to stable titania),<sup>51</sup> and thus, the stability of CuO/TiO<sub>2</sub>-based systems should be improved before possible commercialization.

## V. CONCLUSIONS

In conclusion, small CuO nanoclusters (1–3 nm) were synthesized by radiolysis on the surface of TiO<sub>2</sub>-P25. This modification leads to an enhancement in the photocatalytic activity of TiO<sub>2</sub>-P25

under visible light. Modification of TiO<sub>2</sub> with CuO nanoclusters leads to a good photocatalytic activity under visible light. For photooxidation and degradation of organic pollutants, the best results are obtained with the lowest loading in CuO, while for hydrogen generation, the activity increases with the CuO content. TRMC characterization of modified titania shows strong signals under visible light excitation due to electron transfer from CuO nanoclusters to the conduction band of TiO<sub>2</sub>. This electron injection efficiency depends on the excitation wavelength and loading. However, in aqueous media, the samples are not very stable. In further studies, stabilization of these nanoparticles against oxidation must be considered, for example, by preparation of CuO(core)/TiO<sub>2</sub>(shell) nanostructures. These composite nanomaterials might find other applications, for example, in the gas phase for air treatment, self-cleaning surfaces, or CO<sub>2</sub> reduction.<sup>16</sup> Indeed, CuO has a highly negative CB capable of reducing CO<sub>2</sub> to methanol or formaldehyde.<sup>52</sup> However, if it is irradiated under visible light, electrons from the CB of CuO are going to the CB of TiO<sub>2</sub>. The possibility to reduce CO<sub>2</sub> is reduced. Semiconductors with a narrower bandgap should be used to obtain reduction of CO<sub>2</sub> under visible light, or in the case of titania, irradiation UV should be applied.

## SUPPLEMENTARY MATERIAL

See the [supplementary material](#) for the HRTEM characterization and EDS analysis of CuO nanoparticles, additional XPS analysis and binding energies of the composite CuO<sub>x</sub>/TiO<sub>2</sub>, photocatalytic phenol degradation with cycling, and characterization of the recycled photocatalysts by XPS and STEM analysis.

## ACKNOWLEDGMENTS

Financial support from the CNRS, ECOS-Nord M11-P02 project (CNRS-CONACYT bilateral project), the CONCERT-Japan Joint Call on Efficient Energy Storage (European Commission 31671PB), the COST Nanoalloys, and the CONACYT (Mexico Grant Nos. 106437, 216315, and 356872) is highly acknowledged. In addition, the authors thank the National Laboratory for Nanoscience and Nanotechnology (LINAN-IPICYT) for granting the infrastructure for material characterization and Dr. Mariela Bravo for XPS measurements. M.G.M.-M. acknowledges Campus France for the Eiffel Excellence Scholarship. The authors also acknowledge C’Nano Ile de France, the RTRA Triangle de la Physique, and the ANR project UpPhotoCat for the financial support for the TRMC setup.

## DATA AVAILABILITY

The data that support the findings of this study are available within the article (and its [supplementary material](#)).

## REFERENCES

- <sup>1</sup>K. Hashimoto, H. Irie, and A. Fujishima, *Jpn. J. Appl. Phys., Part 1* **44**, 8269 (2005).
- <sup>2</sup>K. Nakata and A. Fujishima, *J. Photochem. Photobiol., C* **13**, 169 (2012).
- <sup>3</sup>B. Ohtani, *Phys. Chem. Chem. Phys.* **16**, 1788 (2014).
- <sup>4</sup>N.-L. Wu and M.-S. Lee, *Int. J. Hydrogen Energy* **29**, 1601 (2004).



- <sup>5</sup>M. G. Méndez-Medrano, E. Kowalska, A. Lehoux, A. Herissan, B. Ohtani, S. Rau, C. Colbeau-Justin, J. L. Rodríguez-López, and H. Remita, *J. Phys. Chem. C* **120**, 25010 (2016).
- <sup>6</sup>C. Colbeau-Justin, M. Kunst, and D. Huguenin, *J. Mater. Sci.* **38**, 2429 (2003).
- <sup>7</sup>X. Chen and S. S. Mao, *Chem. Rev.* **107**, 2891 (2007).
- <sup>8</sup>J. Yu, Y. Hai, and M. Jaroniec, *J. Colloid Interface Sci.* **357**, 223 (2011).
- <sup>9</sup>D. Liu, Y. Fernández, O. Ola, S. Mackintosh, M. Maroto-Valer, C. M. A. Parlett, A. F. Lee, and J. C. S. Wu, *Catal. Commun.* **25**, 78 (2012).
- <sup>10</sup>Z. Hai, N. E. Kolli, D. B. Uribe, P. Beaunier, M. José-Yacamán, J. Vigneron, A. Etcheberry, S. Sorgues, C. Colbeau-Justin, J. Chen, and H. Remita, *J. Mater. Chem. A* **1**, 10829 (2013).
- <sup>11</sup>S. Linic, P. Christopher, and D. B. Ingram, *Nat. Mater.* **10**, 911 (2011).
- <sup>12</sup>D. Sánchez-Rodríguez, M. G. Méndez Medrano, H. Remita, and V. Escobar-Barrios, *J. Environ. Chem. Eng.* **6**, 1601 (2018).
- <sup>13</sup>N. Helaïli, Y. Bessekhouad, A. Bouguelia, and M. Trari, *J. Hazard. Mater.* **168**, 484 (2009).
- <sup>14</sup>S. Xu and D. D. Sun, *Int. J. Hydrogen Energy* **34**, 6096 (2009).
- <sup>15</sup>M. G. Méndez-Medrano, E. Kowalska, A. Lehoux, A. Herissan, B. Ohtani, D. Bahena, V. Brioso, C. Colbeau-Justin, J. L. Rodríguez-López, and H. Remita, *J. Phys. Chem. C* **120**, 5143 (2016).
- <sup>16</sup>M. G. Méndez-Medrano, E. Kowalska, M. Endo-Kimura, K. Wang, B. Ohtani, D. Bahena Uribe, J. L. Rodríguez-López, and H. Remita, *ACS Appl. Bio Mater.* **2**, 5626 (2019).
- <sup>17</sup>Z. Hai, N. E. Kolli, J. Chen, and H. Remita, *New J. Chem.* **38**, 5279 (2014).
- <sup>18</sup>R. Marschall, *Adv. Funct. Mater.* **24**, 2421 (2014).
- <sup>19</sup>E. Kowalska, M. Janczarek, L. Rosa, S. Juodkazis, and B. Ohtani, *Catal. Today* **230**, 131 (2014).
- <sup>20</sup>M. Janczarek, Z. Wei, M. Endo, B. Ohtani, and E. Kowalska, *J. Photonics Energy* **7**, 012008 (2016).
- <sup>21</sup>M. Jung, J. Scott, Y. H. Ng, Y. Jiang, and R. Amal, *Int. J. Hydrogen Energy* **39**, 12499 (2014).
- <sup>22</sup>Y. Lan, Y. Xie, J. Chen, Z. Hu, and D. Cui, *Chem. Commun.* **55**, 8068 (2019).
- <sup>23</sup>Slamet, H. W. Nasution, E. Purnama, S. Kosela, and J. Gunlazuardi, *Catal. Commun.* **6**, 313 (2005).
- <sup>24</sup>M. Janczarek and E. Kowalska, *Catalysts* **7**, 317 (2017).
- <sup>25</sup>M. Janczarek, K. Wang, and E. Kowalska, *Catalysts* **8**, 240 (2018).
- <sup>26</sup>J. Belloni, M. Mostafavi, H. Remita, J.-L. Marignier, and M.-O. Delcourt, *New J. Chem.* **22**, 1239 (1998).
- <sup>27</sup>R. P. Doherty, J.-M. Krafft, C. Méthivier, S. Casale, H. Remita, C. Louis, and C. Thomas, *J. Catal.* **287**, 102 (2012).
- <sup>28</sup>E. Kowalska, H. Remita, C. Colbeau-Justin, J. Hupka, and J. Belloni, *J. Phys. Chem. C* **112**, 1124 (2008).
- <sup>29</sup>E. Grabowska, A. Zaleska, S. Sorgues, M. Kunst, A. Etcheberry, C. Colbeau-Justin, and H. Remita, *J. Phys. Chem. C* **117**, 1955 (2013).
- <sup>30</sup>J. F. Wishart and B. Rao, *Recent Trends in Radiation Chemistry* (World Scientific, 2010).
- <sup>31</sup>B. Ohtani, O. O. Prieto-Mahaney, D. Li, and R. Abe, *J. Photochem. Photobiol., A* **216**, 179 (2010).
- <sup>32</sup>H. Remita and S. Remita, *Recent Trends in Radiation Chemistry* (World Scientific, 2010), pp. 347–383.
- <sup>33</sup>J. Belloni, *Catal. Today* **113**, 141 (2006).
- <sup>34</sup>C. Ferradini and J. Pucheault, *Biologie de l'Action des Rayonnements Ionisants* (Masson, Paris, 1983).
- <sup>35</sup>J. Khatouri, M. Mostafavi, J. Amblard, and J. Belloni, *Chem. Phys. Lett.* **191**, 351 (1992).
- <sup>36</sup>A. A. Zezin, V. I. Feldman, S. S. Abramchuk, G. V. Danelyan, V. V. Dyo, F. A. Plamper, A. H. E. Müller, and D. V. Pergushov, *Phys. Chem. Chem. Phys.* **17**, 11490 (2015).
- <sup>37</sup>S. Chettibi, N. Kéghouche, Y. Benguedouar, M. M. Bettahar, and J. Belloni, *Catal. Lett.* **143**, 1166 (2013).
- <sup>38</sup>E. Kowalska, O. O. P. Mahaney, R. Abe, and B. Ohtani, *Phys. Chem. Chem. Phys.* **12**, 2344 (2010).
- <sup>39</sup>S.-D. Seo, Y.-H. Jin, S.-H. Lee, H.-W. Shim, and D.-W. Kim, *Nanoscale Res. Lett.* **6**, 397 (2011).
- <sup>40</sup>J. P. Espinós, J. Morales, A. Barranco, A. Caballero, J. P. Holgado, and A. R. González-Elipe, *J. Phys. Chem. B* **106**, 6921 (2002).
- <sup>41</sup>C. C. Chusuei, M. A. Brookshier, and D. W. Goodman, *Langmuir* **15**, 2806 (1999).
- <sup>42</sup>G. L. Chiarello, E. Selli, and L. Forni, *Appl. Catal., B* **84**, 332 (2008).
- <sup>43</sup>G. Colón, M. Maicu, M. C. Hidalgo, and J. A. Navío, *Appl. Catal., B* **67**, 41 (2006).
- <sup>44</sup>Y. Ge, Z. H. Shah, C. Wang, J. Wang, W. Mao, S. Zhang, and R. Lu, *ACS Appl. Mater. Interfaces* **7**, 26437 (2015).
- <sup>45</sup>H. Irie, K. Kamiya, T. Shibanuma, S. Miura, D. A. Tryk, T. Yokoyama, and K. Hashimoto, *J. Phys. Chem. C* **113**, 10761 (2009).
- <sup>46</sup>H. Irie, S. Miura, K. Kamiya, and K. Hashimoto, *Chem. Phys. Lett.* **457**, 202 (2008).
- <sup>47</sup>L. S. Andrade, E. A. Laurindo, R. V. de Oliveira, R. C. Rocha-Filho, and Q. B. Cass, *J. Braz. Chem. Soc.* **17**, 369 (2006).
- <sup>48</sup>J. A. Ortega Méndez, C. R. López, E. Pulido Melián, O. González Díaz, J. M. Doña Rodríguez, D. Fernández Hevia, and M. Macías, *Appl. Catal., B* **147**, 439 (2014).
- <sup>49</sup>M. Ni, M. K. H. Leung, D. Y. C. Leung, and K. Sumathy, *Renewable Sustainable Energy Rev.* **11**, 401 (2007).
- <sup>50</sup>V. Polliotto, S. Livraghi, A. Krukowska, M. V. Dozzi, A. Zaleska-Medynska, E. Selli, and E. Giamello, *ACS Appl. Mater. Interfaces* **10**, 27745 (2018).
- <sup>51</sup>M. Janczarek, M. Endo, D. Zhang, K. Wang, and E. Kowalska, *Materials* **11**, 2069 (2018).
- <sup>52</sup>S. Qin, F. Xin, Y. Liu, X. Yin, and W. Ma, *J. Colloid Interface Sci.* **356**, 257 (2011).